Analysis of Failure Modes in Kesterite Solar Cells

Louis Grenet, Md Abdul, Md Abdoul Aziz Suzon, Fabrice Emieux, Frederic Roux

ACS APPLIED ENERGY MATERIALS

Cite This: ACS Appl. Energy Mater. XXXX, XXX, XXX−XXX

Article

www.acsaem.org

Analysis of Failure Modes in Kesterite Solar Cells

Louis Grenet,*[,†,‡] Md Abdul Aziz Suzon,[†,‡] Fabrice Emieux,[†,‡] and Frédéric Roux[†,‡]

[†]Université Grenoble Alpes, F-38000 Grenoble, France

[‡]CEA, LITEN, 17, rue des Martyrs, F-38054, Cédex 09, Grenoble, France

ABSTRACT: Intense research has been carried out in the past few years to improve efficiencies and understand limitations in kesterite-based solar cells. Despite notable efforts to determine and list the different failure modes affecting the photovoltaic properties of these devices, very few works have tried to quantify and classify the effects of these failure modes. In this study, an exhaustive literature review has first been conducted to determine the different causes leading to limited efficiencies in kesterite devices, with an additional focus on cadmium-free and critical raw material-free devices. Second, an original approach has been employed to quantify the impact of these failure modes on solar cells, based on the evaluation of feedback from 18 scientific experts working on kesterite technology. The result of this survey is analyzed, which allows us to determine what should be the research priority for the community to improve efficiencies and drive kesterite technology to the market.

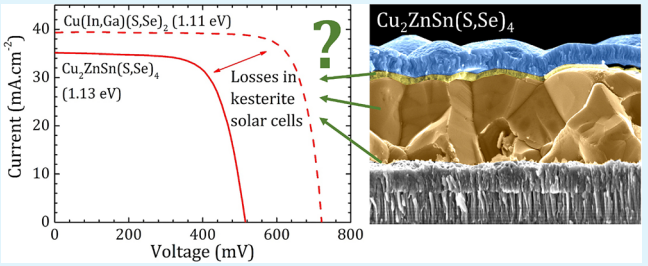

KEYWORDS: *kesterite, CZTSSe solar cells, failure mode analysis, open-circuit voltage deficit, literature review, critical raw material*

1. INTRODUCTION

1.1. Kesterite Solar Cells. Among the thin-film solar cell technologies, $Cu(In,Ga)(S,Se)_2$ (CIGS) and CdTe have already demonstrated power conversion efficiency (PCE) values above 22% at laboratory scale and above 15% for large modules.[1] Industrialization of these technologies is already ongoing, with cumulative production over 4 GWp in 2016.[2] However, both of these technologies contain elements that have been listed by the European Commission as Critical Raw Materials (CRM) for the energy sector,[3,4] namely gallium, indium, and tellurium because of their scarcity in the Earth's crust[5] and their use in other markets. Additionally, progressive implementation worldwide of regulations similar to Restriction on the Use of Hazardous Substances (RoHS) will limit or prevent the use of cadmium in these technologies,[6] both in the absorber layer (CdTe) and in the buffer layer (CdS).

Kesterite semiconductors $Cu_2ZnSn(S,Se)_4$ (CZTSSe) have been identified as promising candidates for thin-film photovoltaic (PV) applications due to their similarities to CIGS materials without containing CRM. To date, a record efficiency of 12.7% has been obtained for a CZTSSe solar cell with a CdS/In_2S_3 buffer layer[7] and 9.0% for a Cd and CRM-free (i.e., without Cd, In, or any CRM) kesterite solar cell.[8]

Due to these limited efficiencies and the gap generally observed between laboratory-scale efficiencies and commercial modules efficiencies,[1] it is felt premature to envisage up-scaling and industrialization of kesterite solar cells. However, evaluating these technologies with an industrially proven results-driven methodology such as Failure Mode and Effect Analysis (FMEA)[9] is of prime importance to correctly assess the challenges relative to the design of the targeted structure and its scalability. Preliminary works on the FMEA of the kesterite absorber have been published in ref 10.

1.2. Scope of the Study. This study focuses on the active part of the CRM-free and Cd and CRM-free kesterite solar cell, which consists of a back electrode (Mo), an absorber material ($Cu_2ZnSn(S,Se)_4$), a buffer layer (without Cd nor CRM), and a window layer (without In). The choice of the substrate and the encapsulant as well as the interconnection of the different solar cells is out of the scope of this study. Although several methods exist for synthesizing the different layers and particularly the absorber layer (precursors deposition via chemical or physical routes, selenization and/or sulfurization, co-evaporation), but also the buffer layer (chemical bath deposition, atomic layer deposition, sputtering), only the final design of the solar cell is considered and not the way to produce it. This focus on a final product is called design FMEA (D-FMEA). The influence of processes to achieve the desired design is out of the scope of the study.

As kesterite-based solar cells and particularly Cd and CRM-free kesterite solar cells are still far from the market, no "standard" device exists. Particularly, no unique buffer layer is commonly chosen. Therefore, different options are considered in this study.

Inventories of the different failure modes occurring in kesterite devices have been gathered in different literature reviews[11−14] and are generally as exhaustive as possible. However, little effort is generally made to quantify and classify

Received: February 8, 2018
Accepted: April 16, 2018
Published: April 16, 2018

DOI: 10.1021/acsaem.8b00194
ACS Appl. Energy Mater. XXXX, XXX, XXX−XXX

these data. This study precisely aims at providing this classification.

1.3. D-FMEA Analysis. D-FMEA is both a qualitative and quantitative technique to determine how an existing or an under-development product might fail and the likely effects of these particular modes of failure.[9] It is based on three figures of merit (FOM) related to the severity, the occurrence, and the non-detection of all failure modes. Each indicator is rated on a 1−10 scale defined in Table 1, and they are multiplied together to give a *risk priority number* (RPN):

$$\text{RPN} = (\text{severity of effect}) \times (\text{likelihood of occurrence}) \times (\text{likelihood of non-detection}) \quad (1)$$

This global value allows to compare the different failure modes and prioritize the ameliorations or modifications that have to be brought to improve the final product. First, actions must address the failure mode with the highest RPN to reduce its value until a second failure mode becomes predominant and so on.

D-FMEA is most often used to analyze an existing product and is thus based on historical data recorded from monitoring system directly on the production line. Particularly, severity and occurrence of failure can be assessed with statistical tools on existing products. In the case of development of new products such as kesterite solar cells, the analysis is more qualitative: a literature review is conducted to determine the different failure modes and to tentatively quantify their FOM. As insufficient data are gathered with this approach, feedback from experts in the domain has been recorded and is summarized in section 2.3.

Table 1. Values Chosen for the Indicators "Severity", "Occurrence", and "Non-detectability"

Severity[a]	
PCE < 20% of the reference technology	10
	9
20% < PCE < 50% of the reference technology	8
	7
	6
50% < PCE < 80% of the reference technology	5
	4
	3
80% < PCE < 90% of the reference technology	2
90% < PCE < 100% of the reference technology	1
Occurrence	
Very high. Almost 100% sure, according to the experience/knowledge of the evaluator, that the type/cause of the failure will happen very frequently; failure almost unavoidable.	10
	9
High. The type/cause of failure happens repeatedly; problematic, non-perfect design.	8
	7
Moderate. The type/cause of the failure happens moderately; advanced design.	6
	5
	4
Low. The probability of the type/cause of failure to happen is low; proven design.	3
	2
Remote. The type/cause of the failure is highly unlikely to happen.	1
Non-detection	
Cannot be detected and/or controlled.	10
Can only be detected indirectly; even if detected, the solution is unknown.	9
Can be detected directly with exotic techniques or a combination of exotic techniques only; if detected, requires thorough study to be overcome.	8
	7
Can be detected with a combination of standard techniques; if detected, requires non-trivial layout or process adjustment to be overcome.	6
	5
Can be detected with standard techniques and corrected with trivial adjustments.	4
	3
	2
Totally under control, always detected, and automatically corrected.	1

[a]PCE can be expected for this technology if only this failure without prior notice. The reference technology for a CZTSSe device is as a state-of-the-art CIGSSe device with a similar bandgap.

2. RESULTS

2.1. Mapping of Fundamental Failures in Cd-Free Kesterite Solar Cells. $Cu_2ZnSn(S,Se)_4$ (CZTSSe) materials are similar to well-established $Cu(In,Ga)(S,Se)_2$ materials and integrated in devices with similar structures.[15] Both materials have tunable bandgaps in the range 1.0−1.5 eV by changing the sulfur on selenium ratio or the indium-on-gallium ratio in CIGSSe solar cells. Similar bandgap variation with cationic substitution can be achieved by replacing tin by germanium in CZTSSe (CZTGSSe). Thus, kesterite as well as chalcopyrite solar cells are theoretically optimum to work as a single junction and to reach the maximum of the Shockley−Queisser (SQ) limit.[16] To illustrate the main limitations of these technologies, the fraction of the SQ limit achieved by all photovoltaic properties (power conversion efficiency, PCE; fill factor, FF; open-circuit voltage, V_{OC}; and short-circuit current, J_{SC}) of the most efficient solar cells as a function of their bandgaps is depicted in Figure 1.

This figure highlights the gap between kesterite and chalcopyrite solar cells. The latter can reach up to 70% of the SQ efficiency limit at intermediate bandgap (1.05−1.2 eV) and 50% for the small ($CuInSe_2$: 0.96 eV) and wide ($Cu(In,Ga)S_2$: 1.57 eV) bandgaps, while $CuInS_2$ and $CuGaSe_2$ are notably underperforming (~40% of SQ limit). The analysis of the most efficient CIGSSe solar cells (PCE > 22%) shows that these devices can exceed 90% of the SQ limit for FF and J_{SC}, while V_{OC} stands in the 80−85% range of this limit.

The picture for kesterite solar cell is totally different. The efficiency of the best devices can only reach 40% of the SQ limit, and this value is further decrease to 30% at wider bandgaps (1.5 eV). The origin of these low efficiencies can be mainly attributed to a limited V_{OC}, which never surpasses 65% of SQ limit, whereas FF and J_{SC} can reach up to 80% of this limit. Introduction of Ge in CZTGSe absorbers has been claimed to improve device properties and particularly V_{OC},[22−26] but Ge-containing devices currently do not outperform their Ge-free counterparts in literature. At low Ge content, FF and V_{OC} are similar to those of Ge-free CZTSSe solar cells but with lower J_{SC}, while at higher content, an additional drop in FF is noticed. As Ge is listed in the CRM,[3] CZTGSe solar cells will be discarded from the further analysis.

As far as Cd and CRM-free CZTSSe solar cells are concerned, the picture is even gloomier, and replacement of the traditional CdS buffer layer systematically lowers V_{OC} and FF, while J_{SC} seems to be less affected. Only two candidates emerge as possibilities to be integrated in kesterite solar cells: Zn(O,OH)[27,28] and ZnSnO.[8,29] Other possibilities such as ZnMgO already used in chalcopyrite solar cells have not been successfully tested so far. CZTSSe/Zn(O,OH) materials

DOI: 10.1021/acsaem.8b00194
ACS Appl. Energy Mater. XXXX, XXX, XXX−XXX

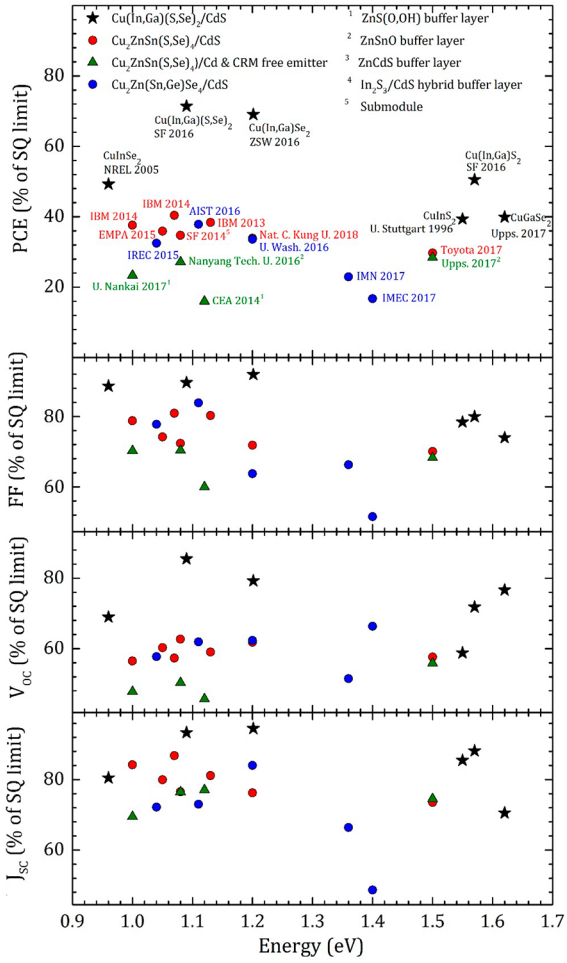

Figure 1. Fraction of the Shockley–Queisser limit (% of SQ limit) achieved by the PV properties of the record CIGSSe, CZTSSe, CZTGSSe, Cd and CRM-free CZTSSe solar cells as a function of their bandgap. Tabulated values of the SQ limit for all parameters from ref 12. PV data and related bandgaps from refs 17–35. Bandgaps are extracted from EQE spectra.

reveals very poor performances (<25% SQ limit) mainly limited by V_{OC} (<50% of SQ limit) and FF (<70% of SQ limit). ZnSnO buffer layers seems to be the most promising candidate with V_{OC} > 50% of SQ limit, while FF and J_{SC} can surpass 70% of SQ limit. Particularly for pure sulfide CZTS absorbers (1.5 eV), solar cells with ZnSnO buffer layers outperform those with the CdS reference one[8] and exhibit similar performances as the state-of-the-art devices.

Different review articles have been published to tentatively explain the efficiency limitation of kesterite solar cells.[11−14] All of them notice first the large V_{OC} deficit (expressed as $E_G/q - V_{OC}$ where E_G is absorber bandgap and q the elemental charge) of kesterite devices followed by low FF and J_{SC} to a lesser extent similarly as the observation made in Figure 1. Starting from these review papers and updated with the most recent literature, a mapping of the fundamental failures in kesterite solar cells has been drawn in Figure 2. The list of failure modes depicted in this mapping is summarized in Table 2. Particular attention has been paid to the influence of Cd and CRM-free buffer layer on device performances since, to the best of our knowledge, no review publication exists on this subject.

V_{OC} deficit in kesterite solar cells can originate either from the bulk material or from its interfaces with supporting layers (buffer layer and Mo back electrode). The two main reasons generally invoked to explain this high V_{OC} deficit are a short minority carrier lifetime and the presence of band tails in the bulk of the absorber material.[36−38] It is worth noticing that both causes cannot be considered at the same level. While band tails (due to electrostatic potential fluctuations or bandgap fluctuations) are directly linked to structural defects in the material (presence of secondary phases in the bulk of the material,[12] Cu/Zn disorder,[39] locally inhomogeneous distribution of the anion,[40] high level of compensated defects[38]), short minority carrier lifetime might be considered as a potential consequence of similar defects. Shockley–Read–Hall (SRH) recombination on point defects in the bulk of the absorber is generally said to be responsible for this short lifetime,[42] but the influence of band tails, grain boundaries, or even interfaces on lifetime is rarely discussed.[13] SRH recombination and tunneling-enhanced recombination,[38] grain boundary recombination,[43−45] low carrier mobility due to defect scattering[46−49] or carrier localization,[50] and insufficient quasi-Fermi-level splitting because of too low carrier density[51] or Fermi-level pinning[52] are mentioned as well as responsible for this V_{OC} deficit. Moreover, the absence of internal electric field cannot counterbalance these poor electronic properties.[53]

V_{OC} deficit of kesterite devices arises not only from the bulk absorber but also from its interfaces with buffer layer and back electrode. A too thick $MoSe_2$ layer can impact device performance.[54] Although decomposition of the absorber in secondary phases on the back electrode has been observed,[55] it has not be claimed to decrease V_{OC}. Front interface is said to be responsible for part of the V_{OC} deficit. Most of the papers discuss the conduction band offset (CBO) between absorber and buffer to form a "spike" at the interface (i.e., conduction band maximum (CBM) of the buffer layer slightly higher (<0.5 eV) than CBM of the absorber layer). For instance CdS is not suitable at high S content in the absorber because of a negative CBO ("cliff" alignment).[12,27] As far as Cd and CRM-free buffer layers are concerned: CBO with ZnO (−0.1 eV) can lead to low V_{OC},[56] ZnSnO has a suitable CBO with CZTSSe for various S content in absorber[27,28] and if CBO with ZnS(O,OH) can be correctly adjusted,[57] inhomogeneity in this buffer layer can drastically reduce V_{OC}.[29] Insufficient buffer coverage can also lead to decreased V_{OC}.[58] The position of Fermi level close to the middle of the hetero-interface due to Fermi-level pinning,[52] the absence of charge inversion at the hetero-interface,[13,59] the high density of interface defects,[59] and the presence of secondary phases at the interface[61,62] are mentioned as well to explain the V_{OC} deficit compared to CIGSSe solar cells. Concerning pure sulfide CZTS absorber, it has been demonstrated that bandgap narrowing at the front interface reduces V_{OC}.[60,63]

As shown in Figure 1, kesterite solar cells and particularly Cd and CRM-free devices suffer as well from reduced FF compared to chalcopyrite ones.[12,14] This lower FF is mainly due to a higher series resistance (R_S):[64] state-of-the-art CZTSSe devices exhibit $R_S \approx 0.7\ \Omega{\cdot}cm^2$[17] compared to $R_S \approx 0.3\ \Omega{\cdot}cm^2$ for CIGSSe devices[31] and a slightly lower shunt resistance (R_{Sh}). This high R_S has been attributed partly to an insufficient bulk absorber conductivity.[65] The explanation can be found in a too low mobility[48] or in the presence of nano-inclusions of ZnSe secondary phases.[69] The influence of a blocking back contact[67] has been revised,[65] but the presence of a thick $MoSe_2$ layer at the back interface[54] or the segregation of ZnSe close to the back interface[68] can imply an additional R_S. Part of this high R_S

DOI: 10.1021/acsaem.8b00194
ACS Appl. Energy Mater. XXXX, XXX, XXX−XXX

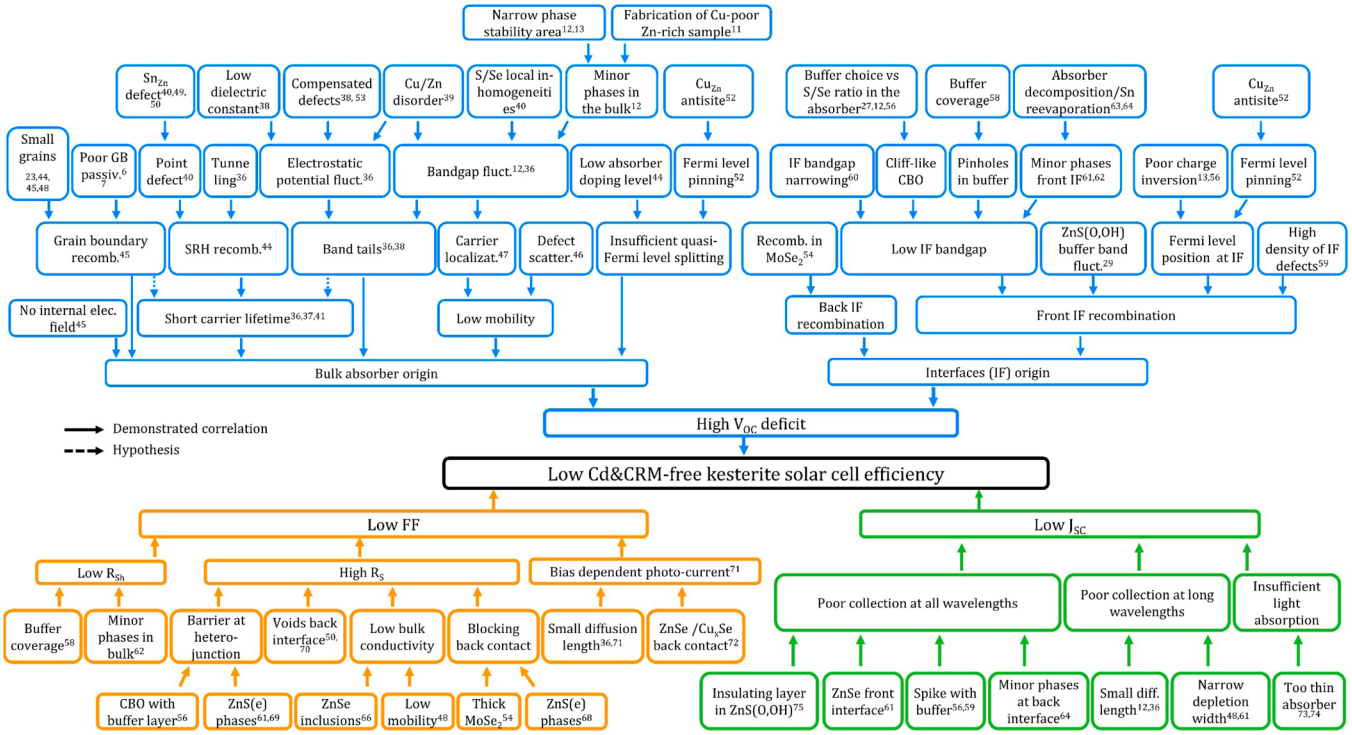

Figure 2. Mapping of the fundamental failures of Cd and CRM-free kesterite solar cells.

can also be linked to a barrier at the hetero-junction due to the presence of a ZnS(e) phase at the surface of the absorber[61,69] or to the CBO with the buffer layer.[56] However, state-of-the-art solar cells with ZnS(O,OH) and ZnSnO buffer layers show similar FF as cells with reference CdS buffer layers.[28,29] It is still not clear whether the presence of voids at the back interface can impact the R_S or not.[50,70]

Another source of FF loss in kesterite devices is linked to low R_{Sh}, which can be due to the presence of secondary phases ($SnSe_2$) in the absorber[62] or to direct contact with the window layer because of insufficient buffer coverage.[58] Interestingly, devices with reasonable R_S and R_{Sh} in the dark can still suffer from low FF under AM1.5 illumination because of bias-dependent current collection.[71] This effect can be related to small minority carrier diffusion length in the absorber[38,74] or to the presence of ZnSe and Cu_xSe close to the back contact.[72]

Last, CZTSSe-based devices suffer from lower J_{SC} than CIGSSe-based ones with similar bandgaps (Figure 1). For pure sulfur CZTS, an insufficient light absorption because of too thin absorbers is noticed.[73,74] The presence of a potential barrier for photocurrent decrease current collection at all wavelengths of the external quantum efficiency (EQE) spectrum.[61] It can be caused by the presence of an insulating ZnSe layer at the top of the absorber,[61] a too high spike at the buffer/absorber interface[56,57] or, in the case of ZnS(O,OH) buffer layers, the formation of a thin ZnS layer at the interface that impedes current collection.[75] The same effect is caused by the presence of secondary phases at the back contact[64] due to absorber decomposition on Mo.[55] Poor photocurrent collection at long wavelengths, which results from small diffusion length in the absorber[12,38] or a too narrow depletion width,[48,61] can be responsible as well for the low J_{SC}.

2.2. Analysis of the Figures of Merit (FOM). The classification of the different failures modes with their respective RPN requires to quantify the figures of merit defined in section 1.3. As no production line for kesterite solar cells can provide reliable historical data to assess *severity*, *occurrence*, and *non-detectability* of the different failure modes determined in section 2.1, an attempt to quantify these FOM has been made from literature. It should be noticed that the values obtained within section 2.2 are only estimations based on the data extracted from literature. A precise quantification of the failure mode on photovoltaic properties is sometimes provided (analysis of V_{OC} losses in refs 38, 40, 41, and 78 for instance), but most of the time, lack of information leads to a rough estimation in Tables 3, 4, and 5. Moreover, contradictory studies can lead to controversial values for part of the FOM, and the impact of some failure modes is still subject to debate.

2.2.1. Severity Quantification in Literature. Potential fluctuations (bandgap or electrostatic fluctuations) due to cationic disorder in kesterite solar cells are one of the main reasons evoked to explain their V_{OC} deficit in literature. Bourdais et al.[40] show that this disorder can account for a maximum deficit of 47 meV (<10% of the V_{OC} deficit) and is not responsible for the majority of the loss. Similarly, S/(S+Se) inhomogeneities at macroscopic and microscopic scales are responsible for less than 30 meV of the V_{OC} deficit. The severity of these failures is relatively low. Additionally, the relative contributions of bandgap and electrostatic potential fluctuations (which originates from Cu/Zn disorder) to band tails are determined to be 70% and 30%, respectively, in ref 76. According to the authors, it explains the absence of correlation between V_{OC} deficit and Cu/Zn disorder as observed elsewhere.[77]

In ref 38, Hages et al. discuss quantitatively the impact of different parameters on voltage limitation at room temperature. While the increase in lifetime from 10 to 100 ns results in a ~150 mV higher V_{OC} (~25% relative gain), a 50% increase in the standard deviation for potential fluctuation would lead to a ~100 mV V_{OC} reduction (~15% relative loss). However,

DOI: 10.1021/acsaem.8b00194
ACS Appl. Energy Mater. XXXX, XXX, XXX−XXX

Table 2. List of the Failure Modes Identified in Figure 2

#	Item/Function	Potential Failure Mode	Potential Effects of Failure	Potential Cause/ Mechanism of Failure
1	Back electrode	Carrier recombination in $MoSe_2$	V_{OC} deficit	Too thick $MoSe_2$
2	Back electrode	Resistive back contact	Low FF	Too thick $MoSe_2$
3	Absorber (back interface)	High R_S	Low FF	Voids at the back interface
4	Absorber (back interface)	High R_S	Low FF	ZnS(e) segregation close to the back contact
5	Absorber (back interface)	Bias dependent photo-current	Low FF	ZnS(e) and Cu_xS(e) close to the back contact due to decomposition on Mo
6	Absorber (bulk)	Low mobility	V_{OC} deficit	Defect scattering
7	Absorber (bulk)	Low mobility	V_{OC} deficit	Carrier localization due to bandgap fluctuations
8	Absorber (bulk)	Short carrier lifetime	V_{OC} deficit	SRH recombination on deep defect in the gap
9	Absorber (bulk)	Short carrier lifetime	V_{OC} deficit	Tunneling assisted recombination
10	Absorber (bulk)	Short carrier lifetime	V_{OC} deficit	Non-radiative carrier recombination through bi-molecular recombination
11	Absorber (bulk)	Grain boundary recombination	V_{OC} deficit	Grains too small & poor grain boundary passivation
12	Absorber (bulk)	Electrostatic potential fluctuations	V_{OC} deficit	Cu/Zn disorder
13	Absorber (bulk)	Electrostatic potential fluctuations	V_{OC} deficit	Very high concentration of compensated defect clusters + low dielectric constant
14	Absorber (bulk)	Bandgap fluctuations	V_{OC} deficit	Presence of secondary phases in the bulk
15	Absorber (bulk)	Bandgap fluctuations	V_{OC} deficit	Cu/Zn disorder
16	Absorber (bulk)	Bandgap fluctuations	V_{OC} deficit	S/Se local inhomogeneities
17	Absorber (bulk)	Absence of internal electric field	V_{OC} deficit	No bandgap gradient
18	Absorber (bulk)	Insufficient quasi fermi-level splitting	V_{OC} deficit	Quasi-fermi level pinning due to high defect (Cu_{Zn}) density
19	Absorber (bulk)	Insufficient quasi fermi-level splitting	V_{OC} deficit	Low doping level in absorber
20	Absorber (bulk)	Short carrier lifetime	Low FF	Non-radiative carrier recombination through bi-molecular recombination
21	Absorber (bulk)	Low R_{Sh}	Low FF	Secondary phases in the bulk ($SnSe_2$)
22	Absorber (bulk)	High R_S	Low FF	Low bulk absorber conductivity
23	Absorber (bulk)	High R_S	Low FF	Presence of ZnSe nano-inclusions
24	Absorber (bulk)	Bias dependent photo-current	Low FF	Small diffusion length in absorber
25	Absorber (bulk)	Poor collection at long wavelengths	Low J_{SC}	Small diffusion length in absorber/absence of bandgap gradient
26	Absorber (bulk)	Poor collection at long wavelengths	Low J_{SC}	Narrow depletion width (too high carrier concentration)
27	Absorber (bulk)	Insufficient light absorption	Low J_{SC}	Sulfur-based absorber too thin
28	Absorber (front interface)	Front interface recombination	V_{OC} deficit	Low interfacial bandgap due to bandgap narrowing (CZTS)
29	Absorber (front interface)	Front interface recombination	V_{OC} deficit	Presence of minor phases at front interface due to absorber decomposition (Sn-loss)
30	Absorber (front interface)	Front interface recombination	V_{OC} deficit	Fermi level position at the middle of hetero-interface (Fermi level pinning)
31	Absorber (front interface)	Front interface recombination	V_{OC} deficit	Poor / no charge inversion in kesterite absorber
32	Absorber (front interface)	Front interface recombination	V_{OC} deficit	High density of non-passivated surface defects
33	Absorber (front interface)	High R_S	Low FF	ZnS(e) secondary phase at the absorber surface
34	Absorber (front interface)	Poor collection at all wavelengths	Low J_{SC}	ZnS(e) secondary phase at the absorber surface
35	Buffer layer - ZnO	Front interface recombination	V_{OC} deficit	Cliff-band alignment with absorber
36	Buffer layer - ZnS(O,OH)	Recombination in buffer layer	V_{OC} deficit	Band fluctuation in buffer layer
37	Buffer layer by sputtering	Front interface recombination	V_{OC} deficit	Insufficient buffer coverage
38	Buffer layer by sputtered	Low R_{Sh}	Low FF	Insufficient buffer coverage
39	Buffer layer - ZnS(O,OH)	High R_S	Low FF	Spike too high at high S content in buffer layer
40	Buffer layer - ZnS(O,OH)	Poor light collection at all wavelengths	Low J_{SC}	Insulating layer formation close to the interface during buffer deposition
41	Buffer layer - ZnS(O,OH)	Poor light collection at all wavelengths	Low J_{SC}	Spike too high at high S content in buffer layer

potential fluctuations in this study account for both bandgap and electrostatic fluctuations, regardless of their origin. Thus, this quantification cannot be attributed unambiguously to a defined failure mode. Suppression of tunneling assisted recombination can only improve V_{OC} by ~7% relative.[38] Hempel et al.[50] discuss the relative influence of low mobility and minority carrier lifetime on device performance. By comparison with chalcopyrite material, they attribute most of the losses to insufficient carrier lifetime, while Gokmen et al.[77] draw an opposite conclusion and incriminate the low mobility. Other studies[41] quantify losses due to low carrier lifetime ("30−50 mV in V_{OC} and 2−4% in absolute efficiency"). Another debated point in literature concerns the responsibility of interface recombination in V_{OC} deficit. While it has been argued to be a major contributor in some studies,[79,80] this point has been questioned in ref 81 and attributed to misinterpretation from data due to non-ideal device behavior.

A rough estimation of the severity of these failure modes from the available data found in literature is given in Table 3.

2.2.2. Occurrence Quantification in Literature. Among the FOM used to classify the failure modes identified in kesterite technology, occurrence is probably the least documented in literature, and if repeatability issues are of prime importance, particularly in view of future industrialization, they are not often discussed at this early stage of development. Thus, assessing occurrence of each failure mode based only on literature review is not possible, and consequently another strategy has been used (see section 2.3).

A very interesting example of process variability is given in ref 72, in which efficiencies of more than 100 devices over almost 3 years are presented. Variation in the results is attributed to ZnSe phase at the back interface leading to bias-dependent photocurrent (failure mode # 5 in Table 2). As most of the cells do not reach the maximum efficiency value, one can argue that occurrence is very high for this particular failure mode.

DOI: 10.1021/acsaem.8b00194
ACS Appl. Energy Mater. XXXX, XXX, XXX−XXX

Table 3. Estimation of the Severity FOM from Literature Review

failure mode	Severity analysis	value	ref
#6, #7	*μ_e is considerably lower for CZTSSe compared to CIGSSe samples whereas τ, as determined by TRPL, is not much different.*	6	78
#7	*The minority carrier mobility is not a real fundamental limit to photocurrent collection and thus device efficiency.*	2	50
#8	*Significant improvements in the V_{OC} are expected ... from improvements in the minority carrier lifetime.*	6	38
	Increasing lifetimes from 2 to 3 ns ... to >100 ns [would gain] 30−50 mV in V_{OC} and 2−4% absolute in efficiency.	5	41
	μ_e is considerably lower for CZTSSe compared to CIGSSe samples whereas τ, as determined by TRPL, is not much different.	2	78
#9	*An improvement in V_{OC} by only ∼7% is estimated for CZTSSe as $E_{00} \rightarrow 0$.*	3	38
#12	*The maximum potential V_{OC} deficit induced by the Cu/Zn disorder is only of 47 meV.*	3	40
	The open-circuit voltage deficit was not affected by the ordering degree.	1	77
#16	*A very negligible fraction (less than 2.5%) of the V_{OC} deficit can be attributed to spatial bandgap fluctuation stemming from anion non-uniformity at the small scale.*	2	40

However, among the tens of solar cells presented in this work, analysis of failure mode is based on the comparison of only two cells, and it is thus not possible to know for certain that it is responsible for all low efficiency cells. This example reveals the difficulty for quantifying this FOM, particularly when no production line and in-line characterization tools are available.

In few cases however, quantification of occurrence is still possible without producing hundreds of samples. Bourdais et al.[40] have shown that CZTSSe samples can have a Cu/Zn disorder ranging from 20% to 100% at room temperature. They demonstrate as well that Cu/Zn disorder does not have an impact on solar cell efficiency in this range of values. However, samples with 0% disorder may exhibit higher efficiencies but are theoretically possible only at 0 K. Thus, an occurrence of 10 can be attributed to failure mode #12 in Table 2, but it is impossible to evaluate simultaneously its severity.

Estimation of the occurrence of these failure modes based on data found in the literature is given in Table 4.

Table 4. Estimation of the Occurrence FOM from Literature Review

failure mode	Occurrence analysis	value	ref
#5	• *[Comparison of] power conversion efficiency of more than 100 devices.* • *We have analyzed the electrical and physical differences between two devices.* • *The reason for the lower efficiency turned out to be a strong bias dependent photocurrent, likely caused by ZnSe secondary phases present at the back contact.*	?	72
#12	*It is not practically possible to reach a degree of Cu−Zn order near S = 1.*	10	76

2.2.3. Non-detectability Quantification in Literature. Short minority carrier lifetime are frequently evoked among the main culprit for V_{OC} deficit in kesterite solar cell.[38,37,41] Time-resolved photoluminescence (TRPL) is mostly used for determining these lifetimes, and values of a few nanoseconds are generally determined. However, Hages et al.[37] have demonstrated that extracting this crucial parameter from decay rate in TRPL signal is not straightforward, and thus, non-detectability FOM related to failure modes #8−#10 in Table 2 are very high (estimated value >8).

The presence of secondary phases in the bulk CZTSSe absorber is also mentioned as a limiting factor for device performances.[12,82] However, detection of part of these minor phases is not straightforward: due to signal overlapping, simple X-ray diffraction (XRD) cannot be used.[82] More sophisticated methods need thus to be employed, such as multiwavelength Raman spectroscopy,[84] X-ray absorption near-edge structure analyses (XANES),[83] and scanning transmission electron microscopy (STEM) in combination with energy-dispersive X-ray spectroscopy[85] or atom probe tomography.[66]

Moreover, detection level of secondary phases can be problematic as well. It has been demonstrated that, even with XRD refinement using Rietveld analysis, amounts of ZnS and Cu_2SnS_3 smaller than 10% and 50%, respectively, are not detectable in CZTS and that Raman spectroscopy using a green laser is unable to detect low levels (30%) of Cu_2SnS_3.[86] Better accuracy for ZnS detection (3%) is obtained using XANES but requires the use of a synchrotron source and works better for S samples than for Se samples.[83]

Based on this literature review, values for the non-detectability indicator have been estimated and summarized in Table 5.

2.2.4. RPN Quantification from Literature. An attempt to calculate RPN for the different failure modes defined in Table 2 has been made from a literature review (severity, occurrence, and non-detectability FOM are reported in Tables 3, 4, and 5, respectively). If the calculation of RPN for some failure modes seems to be possible (for instance, RPN related to low minority carrier lifetime #8 would be very high), two difficulties are encountered in most cases. First, there is an obvious lack of information, which may be partially but not totally completed by a more exhaustive literature review to the best of our knowledge. Particularly, data concerning occurrence are not available for all failure modes. Second, Table 3 shows that contradictory assessment for a single failure mode can be found in literature. For instance, opposite conclusions are drawn to evaluate severity for short minority carrier lifetime and low mobility in ref 77 versus refs 38, 41, and 50. This contradiction either can be linked to different analyses of experimental results or, more fundamentally, can originate from differences in

DOI: 10.1021/acsaem.8b00194
ACS Appl. Energy Mater. XXXX, XXX, XXX−XXX

Table 5. Estimation of the Non-detectability FOM from Literature Review

failure mode	Non-detectability analysis	value	ref
#8–#10	*Various non-ideal absorber properties can dominate the TRPL signal making reliable extraction of the minority carrier lifetime not possible.*	8	37
#4, #5, #23	*Zn-rich phases such as Zn(S,Se) or $Cu_2Sn(S,Se)_3$ X-ray reflections are difficult to separate from kesterite CZTSSe.*	5	82
	GIXRD investigations ... cannot be used to identify sufficiently small amounts of ZnS (<10%) or Cu_2SnS_3 (<50%) phases in a mixed, Cu_2ZnSnS_4 containing sample.	5	86
	• *X-ray absorption near edge structures (XANES) at the sulfur K-edge quantify the ZnS fraction with an absolute accuracy of ±3%.*	8	83
	• *The investigation of the sulfur absorption spectra is preferable.*		

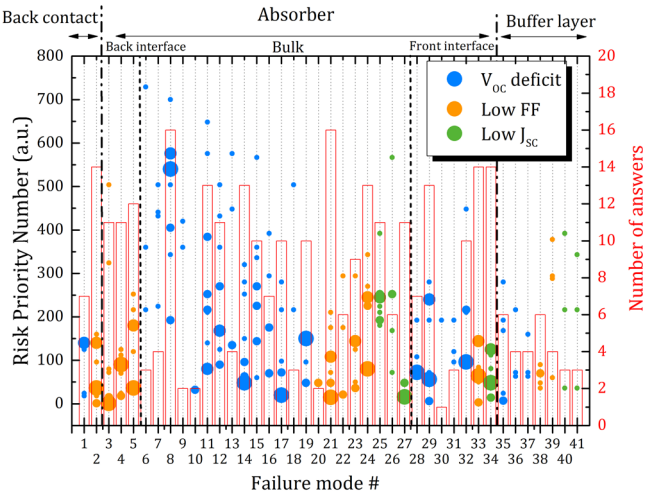

Figure 3. Detailed analysis of the answers to the survey. List of failure modes is given in Table 2. Each point corresponds to an answer: its RPN value is given on the left scale, its size corresponds to the number of people answering, and its colors indicate the effect on PV properties. Red data bars (scale on the right) indicate the number of answers received per failure mode.

samples behavior that have been prepared by various techniques. Hence, it is not possible with literature review to determine the proportion of devices suffering from the different failure modes, and consequently, drawing universal conclusions to determine the origin of efficiency limitations in kesterite devices would be problematic.

Another approach has been developed in the next section to circumvent this difficulty.

2.3. Risk Priority Number. When statistical data from production lines are not available to quantify the RPN for each failure mode, they need to be subjectively determined from knowledge and experience of the experts.[9] As this study has been carried out within the framework of the H2020 STARCELL project, it has been asked to all members of the consortium to evaluate the three FOM (severity, occurrence, and non-detectability) for the failure modes listed in Table 2 through the participation to a survey. This evaluation has been based on their own samples or on their own observations and is not extracted from literature review.

Figure 3 shows all answers to the survey. Some of the partners answered the survey individually (small points), while other groups sent joint answers (from 2 to 5 people; the data point size represents the number of participants). A total of 18 experienced scientists have evaluated the losses in kesterite devices.

First, it is noticeable that each failure mode has not been evaluated by all participants. Particularly failure modes related to the Cd and CRM-free buffer layers did not receive many notations, which can be explained by the limited number of groups working on alternative buffer layers. As far as kesterite absorber or back contact is concerned, the following identified failure modes have been evaluated by less than 30% of participants: low mobility in kesterite absorber, complex recombination scheme (tunneling-assisted recombination or bimolecular recombination), insufficient quasi-Fermi level-splitting, and high concentration of compensated defects along with a low dielectric constant and hetero-interface issues (position of the Fermi level at the hetero-interface and charge inversion in the absorber). On the contrary, the following failure modes have been evaluated by most of the groups (>75% participation): impact of the $MoSe_2$ thickness, short minority carrier lifetime due to SRH recombination, and the presence of secondary phases ($SnSe_2$ in the bulk and ZnSe at the front interface).

Particularly, some failure modes have received a very high RPN only by a small minority of the experts (low mobility issues, quasi-Fermi-level pinning, impact of low dielectric constant, and tunneling-assisted recombination). These evaluations are of course questionable due to the few replies, but a huge effort from the community is requested first and foremost to better understand the related limitations.

Variability in the answers from the participants needs as well to be analyzed. Weighted mean values over the failure modes for each FOM are similar (5.6, 5.4, and 5.3 for severity, occurrence, and non-detectability, respectively), but standard deviation for severity is noticeably higher (2.1) than those for occurrence and non-detectability (1.7 and 1.5, respectively). Thus, it seems that getting a consensus in the community to determine the impact of the most detrimental failure mode will be more challenging than determining their occurrence or detectability.

The variability in the answers can also be studied for each failure mode: the standard deviation divided by the weighted mean value of the RPN (relative standard deviation, RSD) given by all participants has been calculated for each failure mode. Highest values (5.3 and 1.2) have been obtained for failure modes #3 and #2 relative to the impact of back contact (presence of voids and too thick $MoSe_2$) on device series resistance. These high uncertainty has been obtained despite the fact that these failure modes have been evaluated by a majority of participants (11 and 14, respectively). Thus, impact of back contact on series resistance is clearly under debate but is not considered as highly problematic (RPN < 50). Among the most open question (RSD > 1), one can find the origin of parasitic resistances (R_S and R_{Sh} due to minor phases in the bulk: #21 and #22) as well as detrimental behavior at the front interface (presence of secondary phase, #29; insulating layer, #40; or unfavorable band alignment, #35). Impact of S/Se local inhomogeneity (#16) is also subject to debate.

On the other hand, it is agreed (RSD < 0.3, 90% of voters) that low minority carrier lifetime due to SRH recombination in the bulk is one of the most detrimental issues in kesterite devices (RPN = 491).

DOI: 10.1021/acsaem.8b00194
ACS Appl. Energy Mater. XXXX, XXX, XXX−XXX

Figure 4 summarizes the data obtained from the survey. Weighted mean values for each FOM (severity, occurrence, and non-detectability) of all failure modes are shown (gray level, scale on the left), while related RPN are reported on the right. Similarly to Figure 3, the color indicates the effect of the failure mode on the PV properties of the device.

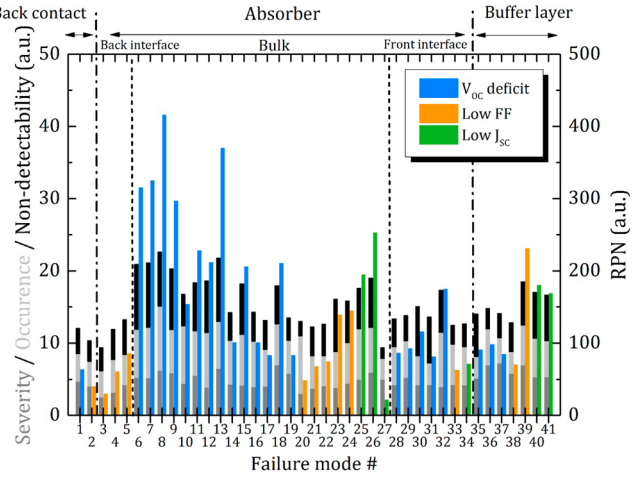

Figure 4. Summary of the answers. List of failure modes is given in Table 2. Mean values obtained for each FOM are shown in gray (scale on the left). Mean values of the RPNs are shown in color bars (same colors as in Figure 3, scale on the right).

Unsurprisingly, failure modes leading to high V_{OC} deficit obtain the highest RPN. Particularly, values of 491 and 370 are found for short minority carrier lifetime (due to SRH recombination, #8) and electrostatic potential fluctuations (due to high concentration compensated defect cluster and low dielectric constant, #13). Solutions to tackle these issues in kesterite solar cells are crucially needed. Impact of grain boundary (#11, RPN = 269) and electrostatic potential fluctuation due to Cu/Zn disorder (#12, RPN = 225) are regarded by a majority of experts as other important causes for the V_{OC} deficit issue.

It must be noted as well that the RPN related to low mobility (due to defect scattering, #6; due to carrier localization in potential fluctuation, #7) are extremely high (values of 420 and 422, respectively). Similarly, insufficient quasi-Fermi-level splitting (#18, RPN = 504) and tunneling-assisted recombination (#9, RPN = 398) are said to be major contributors to the V_{OC} deficit. However, the low participation (<25%) to evaluate these 4 latter cases implies that first efforts should be devoted to correctly understand these issues before trying to care them.

As far as interfaces are concerned, front interface recombination (due to non-passivated surface defects, #32) is identified as well as a major contribution to V_{OC} limitation (RPN = 209), whereas maximum RPN for failure modes related to back contact (#1−#5) does not exceed 100. Thus, at the present stage of technological development, CZTSSe front interface is more problematic than its back interface.

Another point to be highlighted lies in the higher RPN for low J_{SC} than for low FF despite low FF is generally said to be the second reason for limited efficiencies in kesterite devices.[12] Particularly, low J_{SC} resulting from poor collection at long wavelengths (#26 and #25) have been identified as major issues. RPN values of 253 and 219 have been attributed to these failures caused by narrow depletion width (too high carrier concentration) and by small diffusion length in absorber (along with the absence of bandgap gradient). The small diffusion length in absorber is also responsible for bias-dependent photocurrent, leading to limited FF (RPN = 165). Main limitation in FF (RPN = 231) is attributed to unfavorable band alignment for S-rich samples (#39), which is consistent with Figure 1: wide bandgap kesterite devices suffer from low FF compared to Se-based samples.

The 10 most critical failure modes (i.e., with the highest RPN) have been gathered and classified in a descending order in Table 6. It is worth noticing that all of them are contributing to the V_{OC} deficit of the kesterite solar cells and are related to the bulk absorber itself except the failure mode #32 dealing with the front interface. It is important to understand that the values given in Table 6 have not been scientifically demonstrated but have been assessed from the experience of 18 confirmed scientists and reflect the most up-to-date knowledge on kesterite technology. Thus, they need to be considered with care and can be subject to debate, particularly when they are estimated from a low number of responses. However, they give very clear indications where research efforts have to be devoted in order to improve efficiency of CZTSSe solar cells.

Table 6. List of the 10 Failure Modes with the Highest RPN Identified in the Kesterite Technology[a]

#	potential failure mode	potential cause/mechanism of failure	no. of answers	severity	occurrence	non-detectability	RPN
#8	short carrier lifetime	SRH recombination on deep defect in the gap	14	7.3	8.4	7.9	478
#18	insufficient quasi-Fermi-level splitting	quasi-Fermi-level pinning due to high defect (Cu_{Zn}) density	3	8.6	5.7	9.3	455
#6	low mobility	defect scattering	3	7.0	6.7	9.0	420
#13	electrostatic potential fluctuations	very high concentration of compensated defect clusters + low dielectric constant	4	6.8	7.0	8.7	410
#7	low mobility	carrier localization due to bandgap fluctuations	4	6.6	7.0	8.8	407
#9	short carrier lifetime	tunneling assisted recombination	2	7.8	6.0	8.3	384
#11	grain boundary recombination	grains too small and poor grain boundary passivation	13	6.6	6.4	7.1	297
#32	front interface recombination	high density of non-passivated surface defects	8	5.8	7.0	7.2	291
#12	electrostatic potential fluctuations	Cu/Zn disorder	11	5.3	7.7	6.8	273
#15	bandgap fluctuations	Cu/Zn disorder	10	5.3	7.3	6.6	253

[a]All these failure modes impact the V_{OC} deficit of the solar cells.

DOI: 10.1021/acsaem.8b00194
ACS Appl. Energy Mater. XXXX, XXX, XXX−XXX

3. CONCLUSIONS

This study describes an FMEA study of kesterite solar cells with an additional focus on Cd and CRM-free devices. A systematic and exhaustive literature review has been conducted to determine the origin of the photovoltaic limitations in kesterite devices including those with alternative buffer layer. A particular attention has been paid to the demonstration of the causes of each failure mode. However, the physical origin of short minority carrier lifetime, which is said to be responsible for a significant part of the V_{OC} deficit, is barely discussed.

As this literature review does not allow us to quantify the FOM related to these failure modes and thus does not allow us to classify them, an alternative solution has been chosen. A survey has been distributed within the consortium of the STARCELL project; an evaluation of the kesterite devices failure modes has been made by 18 scientific experts. This original feedback on concrete experience allows us to quantify and classify the limitations in CZTSSe solar cells.

Short minority carrier lifetime and presence of band tails are mostly identified as culprits for the V_{OC} deficit, which is the main limitation for device efficiency. However, few contributions have noticed as well the possible very detrimental impact of insufficient quasi-Fermi-level splitting and low carrier mobility, which must be subject of high attention. Last, a consensus emerges on the fact that limitations in kesterite technologies arise from the bulk absorber itself rather than from its interfaces.

AUTHOR INFORMATION

Corresponding Author

*E-mail: louis.grenet@cea.fr.

ORCID

Louis Grenet: 0000-0003-0580-2929

Notes

The authors declare no competing financial interest.

ACKNOWLEDGMENTS

This research was supported by the H2020 Programme under the project STARCELL (H2020-NMBP-03-2016-720907) and the Laboratoire d'excellence LANEF in Grenoble (ANR-10-LABX-51-01). The authors are particularly grateful to members of the STARCELL consortium for their valuable contribution to this study.

REFERENCES

(1) Green, M. A.; Hishikawa, Y.; Warta, W.; Dunlop, E. D.; Levi, D. H.; Hohl-Ebinger, J.; Ho-Baillie, A. W. Solar cell efficiency tables (version 50). *Prog. Photovoltaics* **2017**, *25* (7), 668−676.

(2) Burger, B.; Kiefer, K.; Kost, C.; Nold, S.; Philipps, S.; Preu, R.; Rentsch, J.; Schlegl, T.; Stryi-Hipp, G.; Willeke, G.; Wirth, H.; Warmuth, W. *Photovoltaics Report*; Frauhofer ISE, Feb 26, 2018; https://www.ise.fraunhofer.de/content/dam/ise/de/documents/publications/studies/Photovoltaics-Report.pdf.

(3) Ad-Hoc Working Group on Defining Critical Raw Materials. *Report on Critical Raw Materials for the EU*; European Commission, May 2014; http://www.catalysiscluster.eu/wp/wp-content/uploads/2015/05/2014_Critical-raw-materials-for-the-EU-2014.pdf.

(4) Moss, R. L.; Tzimas, E.; Willis, P.; Arendorf, J.; Thompson, P.; Chapman, A.; Morley, N.; Sims, E.; Bryson, R.; Pearson, J.; Tercero-Espinoza, L. Critical Metals in the Path Towards the Decarbonisation of the EU Energy Sector. Assessing Rare Metals As Supply-Chain Bottlenecks in Low-Carbon Energy Technologies. *JRC Scientific and Policy Reports*, EUR 25994; Joint Research Center, European Commission, 2013; https://setis.ec.europa.eu/sites/default/files/reports/JRC-report-Critical-Metals-Energy-Sector.pdf

(5) Wedepohl, K. H. The composition of the continental crust. *Geochim. Cosmochim. Acta* **1995**, *59* (7), 1217−1232.

(6) Horn, D. A. The international development of RoHS. In Technologies for Sustainability (SusTech). *Proc. IEEE Conference* **2016**, 34−38.

(7) Kim, J.; Hiroi, H.; Todorov, T. K.; Gunawan, O.; Kuwahara, M.; Gokmen, T.; Nair, D.; Hopstaken, M.; Shin, B.; Lee, Y. S.; Wang, W. J.; Sugimoto, H.; Mitzi, D. B. High efficiency $Cu_2ZnSn(S,Se)_4$ solar cells by applying a double In_2S_3/CdS emitter. *Adv. Mater.* **2014**, *26* (44), 7427−7431.

(8) Ericson, T.; Larsson, F.; Törndahl, T.; Frisk, C.; Larsen, J.; Kosyak, V.; Hägglund, C.; Li, S.; Platzer-Björkman, C. Zinc-Tin-Oxide Buffer Layer and Low Temperature Post Annealing Resulting in a 9.0% Efficient Cd-Free Cu_2ZnSnS_4 Solar Cell. *Sol. RRL* **2017**, *1* (5), 1700001.

(9) Snee, R. D.; Rodebaugh, W. F. Failure Modes and Effects Analysis. *Encyclopedia of Statistics in Quality and Reliability*; Wiley: Weinheim, 2008.

(10) Aninat, R.; Quesada-Rubio, L. E.; Sanchez-Cortezon, E.; Delgado-Sanchez, J. M. Mapping and comparison of the shortcomings of kesterite absorber layers, and how they could affect industrial scalability. *Thin Solid Films* **2017**, *633*, 146−150.

(11) Delbos, S. Kësterite thin films for photovoltaics: a review. *EPJ Photovoltaics* **2012**, *3*, 35004.

(12) Siebentritt, S. Why are kesterite solar cells not 20% efficient? *Thin Solid Films* **2013**, *535*, 1−4.

(13) Polizzotti, A.; Repins, I. L.; Noufi, R.; Wei, S. H.; Mitzi, D. B. The state and future prospects of kesterite photovoltaics. *Energy Environ. Sci.* **2013**, *6*, 3171−3182.

(14) Liu, X.; Feng, Y.; Cui, H.; Liu, F.; Hao, X.; Conibeer, G.; Mitzi, D. B.; Green, M. The current status and future prospects of kesterite solar cells: a brief review. *Prog. Photovoltaics* **2016**, *24* (6), 879−898.

(15) Repins, I.; Vora, N.; Beall, C.; Wei, S.-H.; Yan, Y.; Romero, M.; Teeter, G.; Du, H.; To, B.; Young, M.; Noufi, R. Kesterites and chalcopyrites: a comparison of close cousins. *MRS Online Proc. Libr.* **2011**, *1324*, 844.

(16) Rühle, S. Tabulated values of the Shockley−Queisser limit for single junction solar cells. *Sol. Energy* **2016**, *130*, 139−147.

(17) Wang, W.; Winkler, M. T.; Gunawan, O.; Gokmen, T.; Todorov, T. K.; Zhu, Y.; Mitzi, D. B. Device Characteristics of CZTSSe Thin-Film Solar Cells with 12.6% Efficiency. *Adv. Energy Mater.* **2014**, *4*, 1301465.

(18) Kato, T.; Sakai, N.; Sugimoto, H. Efficiency improvement of $Cu_2ZnSn(S,Se)_4$ submodule with graded bandgap and reduced backside ZnS segregation. *Proc. 40th IEEE PVSC* **2014**, 0844−0846.

(19) Haass, S. G.; Diethelm, M.; Werner, M.; Bissig, B.; Romanyuk, Y. E.; Tiwari, A. N. 11.2% Efficient Solution Processed Kesterite Solar Cell with a Low Voltage Deficit. *Adv. Energy Mater.* **2015**, *5*, 1500712.

(20) Lee, Y. S.; Gershon, T.; Gunawan, O.; Todorov, T. K.; Gokmen, T.; Virgus, Y.; Guha, S. $Cu_2ZnSnSe_4$ Thin-Film Solar Cells by Thermal Co-evaporation with 11.6% Efficiency and Improved Minority Carrier Diffusion Length. *Adv. Energy Mater.* **2015**, *5* (7), 1401372.

(21) Tajima, S.; Umehara, M.; Hasegawa, M.; Mise, T.; Itoh, T. Cu_2ZnSnS_4 photovoltaic cell with improved efficiency fabricated by high-temperature annealing after CdS buffer-layer deposition. *Prog. Photovoltaics* **2017**, *25* (1), 14−22.

(22) Kim, S.; Kim, K. M.; Tampo, H.; Shibata, H.; Niki, S. Improvement of voltage deficit of Ge-incorporated kesterite solar cell with 12.3% conversion efficiency. *Appl. Phys. Express* **2016**, *9* (10), 102301.

(23) Giraldo, S.; Neuschitzer, M.; Thersleff, T.; López-Marino, S.; Sánchez, Y.; Xie, H.; Colina, M.; Placidi, M.; Pistor, P.; Izquierdo-Roca, V.; Leifer, K.; Pérez-Rodriguez, A.; Saucedo, E. Large Efficiency Improvement in $Cu_2ZnSnSe_4$ Solar Cells by Introducing a Superficial Ge Nanolayer. *Adv. Energy Mater.* **2015**, *5*, 1501070.

DOI: 10.1021/acsaem.8b00194
ACS Appl. Energy Mater. XXXX, XXX, XXX−XXX

(24) Collord, A.; Hillhouse, H. Germanium Alloyed Kesterite Solar Cells with Low Voltage Deficits. *Chem. Mater.* **2016**, *28* (7), 2067−2073.
(25) Sahayaraj, S.; Brammertz, G.; Vermang, B.; Schnabel, T.; Ahlswede, E.; Huang, Z.; Ranjbar, S.; Meuris, M.; Vleugels, J.; Poortmans, J. S. Optoelectronic properties of thin film $Cu_2ZnGeSe_4$ solar cells. *Sol. Energy Mater. Sol. Cells* **2017**, *171*, 136−141.
(26) Choubrac, L.; Brammertz, G.; Arzel, L.; Harel, S.; Assmann, L.; Meuris, M.; Vermang, B.; Barreau, N., unpublished.
(27) Grenet, L.; Grondin, P.; Coumert, K.; Karst, N.; Emieux, F.; Roux, F.; Fillon, R.; Altamura, G.; Fournier, H.; Faucherand, P.; Perraud, S. Experimental evidence of light soaking effect in Cd-free $Cu_2ZnSn(S,Se)_4$-based solar cells. *Thin Solid Films* **2014**, *564*, 375−378.
(28) Li, X.; Su, Z.; Venkataraj, S.; Batabyal, S. K.; Wong, L. H. 8.6% Efficiency CZTSSe solar cell with atomic layer deposited Zn-Sn-O buffer layer. *Sol. Energy Mater. Sol. Cells* **2016**, *157*, 101−107.
(29) Li, J.; Liu, X.; Liu, W.; Wu, L.; Ge, B.; Lin, S.; Gao, S.; Zhou, Z.; Liu, F.; Sun, Y.; Ao, J.; Zhu, H.; Mai, Y.; Zhang, Y. Restraining the Band Fluctuation of CBD-Zn (O, S) Layer: Modifying the Hetero-Junction Interface for High Performance $Cu_2ZnSnSe_4$ Solar Cells With Cd-Free Buffer Layer. *Sol. RRL* **2017**, *1*, 1700075.
(30) Jackson, P.; Wuerz, R.; Hariskos, D.; Lotter, E.; Witte, W.; Powalla, M. Effects of heavy alkali elements in $Cu(In,Ga)Se_2$ solar cells with efficiencies up to 22.6%. *Phys. Status Solidi RRL* **2016**, *10* (8), 583−586.
(31) Hiroi, H.; Iwata, Y.; Adachi, S.; Sugimoto, H.; Yamada, A. New world-record efficiency for pure-sulfide $Cu(In,Ga)S_2$ thin-film solar cell with Cd-free buffer layer via KCN-free process. *IEEE J. Photovoltaics* **2016**, *6* (3), 760−763.
(32) Kamada, R.; Yagioka, T.; Adachi, S.; Handa, A.; Tai, K. F.; Kato, T.; Sugimoto, H. New world record $Cu(In,Ga)(Se,S)_2$ thin film solar cell efficiency beyond 22%. *Proc. 43rd IEEE PVSC* **2016**, 1287−1291.
(33) AbuShama, J.; Noufi, R.; Johnston, S.; Ward, S.; Wu, X. Improved Performance in $CuInSe_2$ and Surface Modified $CuGaSe_2$ Solar Cells. *Proc. 31st IEEE PVSC* **2005**, 299−302.
(34) Braunger, D.; Durr, T.; Hariskos, D.; Koble, C.; Walter, T.; Wieser, N.; Schock, H. W. Improved open circuit voltage in $CuInS_2$-based solar cells. *Proc. 25th IEEE PVSC* **1996**, 1001−1004.
(35) Larsson, F.; Nilsson, N. S.; Keller, J.; Frisk, C.; Kosyak, V.; Edoff, M.; Törndahl, T. Record 1.0 V open-circuit voltage in wide band gap chalcopyrite solar cells. *Prog. Photovoltaics* **2017**, *25* (9), 755−763.
(36) Hages, C. J.; Carter, N. J.; Agrawal, R.; Unold, T. Generalized current-voltage analysis and efficiency limitations in non-ideal solar cells: Case of $Cu_2ZnSn(S_xSe_{1-x})_4$ and $Cu_2Zn(Sn_yGe_{1-y})(S_xSe_{1-x})_4$. *J. Appl. Phys.* **2014**, *115* (23), 234504.
(37) Hages, C. J.; Redinger, A.; Levcenko, S.; Hempel, H.; Koeper, M. J.; Agrawal, R.; Greiner, D.; Kaufmann, C. A.; Unold, T. Identifying the Real Minority Carrier Lifetime in Nonideal Semiconductors: A Case Study of Kesterite Materials. *Adv. Energy Mater.* **2017**, *7*, 1700167.
(38) Gokmen, T.; Gunawan, O.; Todorov, T. K.; Mitzi, D. B. Band tailing and efficiency limitation in kesterite solar cells. *Appl. Phys. Lett.* **2013**, *103* (10), 103506.
(39) Scragg, J. J.; Larsen, J. K.; Kumar, M.; Persson, C.; Sendler, J.; Siebentritt, S.; Platzer Björkman, C. Cu−Zn disorder and band gap fluctuations in $Cu_2ZnSn(S, Se)_4$: Theoretical and experimental investigations. *Phys. Status Solidi B* **2016**, *253*, 189.
(40) Bourdais, S.; Choné, C.; Delatouche, B.; Jacob, A.; Larramona, G.; Moisan, C.; Lafond, A.; Donatini, F.; Rey, G.; Siebentritt, S.; Walsh, A.; Dennler, G. Is the Cu/Zn disorder the main culprit for the voltage deficit in kesterite solar cells? *Adv. Energy Mater.* **2016**, *6* (12), 1502276.
(41) Repins, I. L.; Moutinho, H.; Choi, S. G.; Kanevce, A.; Kuciauskas, D.; Dippo, P.; Beall, C. L.; Carapella, J.; DeHart, C.; Huang, B.; Wei, S. H. Indications of short minority-carrier lifetime in kesterite solar cells. *J. Appl. Phys.* **2013**, *114* (8), 084507.
(42) Guglietta, G. W.; Choudhury, K. R.; Caspar, J. V.; Baxter, J. B. Employing time-resolved terahertz spectroscopy to analyze carrier dynamics in thin-film $Cu_2ZnSn(S,Se)_4$ absorber layers. *Appl. Phys. Lett.* **2014**, *104* (25), 253901.
(43) Sardashti, K.; Haight, R.; Gokmen, T.; Wang, W.; Chang, L. Y.; Mitzi, D. B.; Kummel, A. C. Impact of Nanoscale Elemental Distribution in High-Performance Kesterite Solar Cells. *Adv. Energy Mater.* **2015**, *5* (10), 1402180.
(44) Li, J. B.; Chawla, V.; Clemens, B. M. Investigating the role of grain boundaries in CZTS and CZTSSe thin film solar cells with scanning probe microscopy. *Adv. Mater.* **2012**, *24*, 720−723.
(45) Jiang, C.-S.; Repins, I. L.; Beall, C.; Moutinho, H.; Ramanathan, K.; Al-Jassim, M. Investigation of micro-electrical properties of $Cu_2ZnSnSe_4$ thin films using scanning probe microscopy. *Sol. Energy Mater. Sol. Cells* **2015**, *132*, 342−347.
(46) Nagaoka, A.; Miyake, H.; Taniyama, T.; Kakimoto, K.; Nose, Y.; Scarpulla, M. A.; Yoshino, K. Effects of sodium on electrical properties in Cu_2ZnSnS_4 single crystal. *Appl. Phys. Lett.* **2014**, *104*, 152101.
(47) Hempel, H.; Redinger, A.; Repins, I.; Moisan, C.; Larramona, G.; Dennler, G.; Handwerg, M.; Fischer, S. F.; Eichberger, R.; Unold, T. Intragrain charge transport in kesterite thin films—Limits arising from carrier localization. *J. Appl. Phys.* **2016**, *120* (17), 175302.
(48) Gunawan, O.; Gokmen, T.; Mitzi, D. B. Suns-V_{OC} characteristics of high performance kesterite solar cells. *J. Appl. Phys.* **2014**, *116* (8), 084504.
(49) Larramona, G.; Levcenko, S.; Bourdais, S.; Jacob, A.; Choné, C.; Delatouche, B.; Moisan, C.; Just, J.; Unold, T.; Dennler, G. Fine-Tuning the Sn Content in CZTSSe Thin Films to Achieve 10.8% Solar Cell Efficiency from Spray-Deposited Water−Ethanol-Based Colloidal Inks. *Adv. Energy Mater.* **2015**, *5* (24), 1501404.
(50) López-Marino, S.; Placidi, M.; Pérez-Tomás, A.; Llobet, J.; Izquierdo-Roca, V.; Fontané, X.; Fairbrother, A.; Espindola-Rodriguez, M.; Sylla, D.; Perez-Rodriguez, A.; Saucedo, E. Inhibiting the absorber/Mo-back contact decomposition reaction in $Cu_2ZnSnSe_4$ solar cells: the role of a ZnO intermediate nanolayer. *J. Mater. Chem. A* **2013**, *1* (29), 8338−8343.
(51) Li, J. V.; Kuciauskas, D.; Young, M. R.; Repins, I. L. Effects of sodium incorporation in Co-evaporated $Cu_2ZnSnSe_4$ thin-film solar cells. *Appl. Phys. Lett.* **2013**, *102*, 163905.
(52) Yuan, Z. K.; Chen, S.; Xiang, H.; Gong, X. G.; Walsh, A.; Park, J. S.; Repins, I. L.; Wei, S. H. Engineering solar cell absorbers by exploring the band alignment and defect disparity: the case of Cu-and Ag-based kesterite compounds. *Adv. Funct. Mater.* **2015**, *25* (43), 6733−6743.
(53) Yin, L.; Cheng, G.; Feng, Y.; Li, Z.; Yang, C.; Xiao, X. Limitation factors for the performance of kesterite Cu_2ZnSnS_4 thin film solar cells studied by defect characterization. *RSC Adv.* **2015**, *5* (50), 40369−40374.
(54) Shin, B.; Zhu, Y.; Bojarczuk, N. A.; Jay Chey, S.; Guha, S. Control of an interfacial $MoSe_2$ layer in $Cu_2ZnSnSe_4$ thin film solar cells: 8.9% power conversion efficiency with a TiN diffusion barrier. *Appl. Phys. Lett.* **2012**, *101* (5), 053903.
(55) Scragg, J. J.; Watjen, J. T.; Edoff, M.; Ericson, T.; Kubart, T.; Platzer-Björkman, C. A detrimental reaction at the molybdenum back contact in $Cu_2ZnSn(S,Se)_4$ thin-film solar cells. *J. Am. Chem. Soc.* **2012**, *134* (47), 19330−19333.
(56) Barkhouse, D. A. R.; Haight, R.; Sakai, N.; Hiroi, H.; Sugimoto, H.; Mitzi, D. B. Cd-free buffer layer materials on $Cu_2ZnSn(S_xSe_{1-x})_4$: Band alignments with ZnO, ZnS, and In_2S_3. *Appl. Phys. Lett.* **2012**, *100* (19), 193904.
(57) Neuschitzer, M.; Lienau, K.; Guc, M.; Barrio, L. C.; Haass, S.; Prieto, J. M.; Sanchez, Y.; Espindola-Rodriguez, M.; Romanyuk, Y.; Perez-Rodriguez, A.; Izquierdo-Roca, V.; Saucedo, E. Towards high performance Cd-free CZTSe solar cells with a ZnS(O,OH) buffer layer: the influence of thiourea concentration on chemical bath deposition. *J. Phys. D: Appl. Phys.* **2016**, *49* (12), 125602.
(58) Kim, J.; Park, C.; Pawar, S. M.; Inamdar, A. I.; Jo, Y.; Han, J.; Hong, J.; Park, Y. S.; Kim, D.-Y.; Jung, W.; Kim, H.; Im, H.

DOI: 10.1021/acsaem.8b00194
ACS Appl. Energy Mater. XXXX, XXX, XXX−XXX

Optimization of sputtered ZnS buffer for Cu_2ZnSnS_4 thin film solar cells. *Thin Solid Films* **2014**, *566*, 88−92.
(59) Li, J.; Mitzi, D. B.; Shenoy, V. B. Structure and electronic properties of grain boundaries in earth-abundant photovoltaic absorber $Cu_2ZnSnSe_4$. *ACS Nano* **2011**, *5* (11), 8613−8619.
(60) Crovetto, A.; Palsgaard, M. L.; Gunst, T.; Markussen, T.; Stokbro, K.; Brandbyge, M.; Hansen, O. Interface band gap narrowing behind open circuit voltage losses in Cu_2ZnSnS_4 solar cells. *Appl. Phys. Lett.* **2017**, *110* (8), 083903.
(61) López-Marino, S.; Sánchez, Y.; Placidi, M.; Fairbrother, A.; Espindola-Rodríguez, M.; Fontané, X.; Izquierdo-Roca, V.; Lopez-Garcia, J.; Calvo-Barrio, L.; Perez-Rodriguez, A.; Saucedo, E. ZnSe Etching of Zn-Rich $Cu_2ZnSnSe_4$: An Oxidation Route for Improved Solar-Cell Efficiency. *Chem. - Eur. J.* **2013**, *19* (44), 14814−14822.
(62) Temgoua, S.; Bodeux, R.; Naghavi, N.; Delbos, S. Effects of $SnSe_2$ secondary phases on the efficiency of $Cu_2ZnSn(S_xSe_{1-x})_4$ based solar cells. *Thin Solid Films* **2015**, *582*, 215−219.
(63) Weber, A.; Mainz, R.; Schock, H. W. On the Sn loss from thin films of the material system Cu−Zn−Sn−S in high vacuum. *J. Appl. Phys.* **2010**, *107* (1), 013516.
(64) Scragg, J. J.; Kubart, T.; Wätjen, J. T.; Ericson, T.; Linnarsson, M. K.; Platzer-Björkman, C. Effects of back contact instability on Cu_2ZnSnS_4 devices and processes. *Chem. Mater.* **2013**, *25*, 3162−3171.
(65) Gunawan, O.; Gokmen, T.; Warren, C. W.; Cohen, J. D.; Todorov, T. K.; Barkhouse, D. A. R.; Bag, S.; Tang, J.; Shin, B.; Mitzi, D. B. Electronic properties of the $Cu_2ZnSn(Se,S)_4$ absorber layer in solar cells as revealed by admittance spectroscopy and related methods. *Appl. Phys. Lett.* **2012**, *100*, 253905.
(66) Schwarz, T.; Cojocaru-Mirédin, O.; Choi, P.; Mousel, M.; Redinger, A.; Siebentritt, S.; Raabe, D. Atom probe study of $Cu_2ZnSnSe_4$ thin-films prepared by co-evaporation and post-deposition annealing. *Appl. Phys. Lett.* **2013**, *102* (4), 042101.
(67) Gunawan, O.; Todorov, T. K.; Mitzi, D. B. Loss mechanisms in hydrazine-processed $Cu_2ZnSn(Se,S)_4$ solar cells. *Appl. Phys. Lett.* **2010**, *97*, 233506.
(68) Redinger, A.; Hönes, K.; Fontané, X.; Izquierdo-Roca, V.; Saucedo, E.; Valle, N.; Perez-Rodriguez, A.; Siebentritt, S. Detection of a ZnSe secondary phase in coevaporated $Cu_2ZnSnSe_4$ thin films. *Appl. Phys. Lett.* **2011**, *98* (10), 101907.
(69) Redinger, A.; Mousel, M.; Wolter, M. H.; Valle, N.; Siebentritt, S. Influence of S/Se ratio on series resistance and on dominant recombination pathway in $Cu_2ZnSn(SSe)_4$ thin film solar cells. *Thin Solid Films* **2013**, *535*, 291−295.
(70) Brammertz, G.; Buffière, M.; Oueslati, S.; ElAnzeery, H.; Messaoud, K. B.; Sahayaraj, S.; Köble, C.; Meuris, M.; Poortmans, J. Characterization of defects in 9.7% efficient $Cu_2ZnSnSe_4$-CdS-ZnO solar cells. *Appl. Phys. Lett.* **2013**, *103*, 163904.
(71) Grenet, L.; Fillon, R.; Altamura, G.; Fournier, H.; Emieux, F.; Faucherand, P.; Perraud, S. Analysis of photovoltaic properties of $Cu_2ZnSn(S,Se)_4$-based solar cells. *Sol. Energy Mater. Sol. Cells* **2014**, *126*, 135−142.
(72) Brammertz, G.; Buffière, M.; Verbist, C.; Oueslati, S.; Bekaert, J.; ElAnzeery, H.; Messaoud, K. B.; Sahayaraj, S.; Batuk, M.; Hadermann, J.; Köble, C.; Meuris, M.; Poortmans, J. Process variability in $Cu_2ZnSnSe_4$ solar cell devices: Electrical and structural investigations. *Proc. 42nd IEEE PVSC* **2015**, 1−4.
(73) Shin, B.; Gunawan, O.; Zhu, Y.; Bojarczuk, N. A.; Chey, S. J.; Guha, S. Thin film solar cell with 8.4% power conversion efficiency using an earth-abundant Cu_2ZnSnS_4 absorber. *Prog. Photovoltaics* **2013**, *21*, 72−76.
(74) Sugimoto, H.; Hiroi, H.; Sakai, N.; Muraoka, S.; Katou, T. Over 8% efficiency Cu_2ZnSnS_4 submodules with ultra-thin absorber. *Proc. 38th IEEE PVSC* **2012**, 2997−3000.
(75) Gautron, E.; Buffière, M.; Harel, S.; Assmann, L.; Arzel, L.; Brohan, L.; Kessler, J.; Barreau, N. Microstructural characterization of chemical bath deposited and sputtered Zn(O,S) buffer layers. *Thin Solid Films* **2013**, *535*, 175−179.
(76) Rey, G.; Larramona, G.; Bourdais, S.; Choné, C.; Delatouche, B.; Jacob, A.; Dennler, G.; Siebentritt, S. On the origin of band-tails in kesterite. *Sol. Energy Mater. Sol. Cells* **2018**, *179*, 142−151.
(77) Rey, G.; Weiss, T. P.; Sendler, J.; Finger, A.; Spindler, C.; Werner, F.; Melchiorre, M.; Hála, M.; Guennou, M.; Siebentritt, S. Ordering kesterite improves solar cells: A low temperature post-deposition annealing study. *Sol. Energy Mater. Sol. Cells* **2016**, *151*, 131−138.
(78) Gokmen, T.; Gunawan, O.; Mitzi, D. B. Minority carrier diffusion length extraction in $Cu_2ZnSn(Se,S)_4$ solar cells. *J. Appl. Phys.* **2013**, *114* (11), 114511.
(79) Todorov, T. K.; Tang, J.; Bag, S.; Gunawan, O.; Gokmen, T.; Zhu, Y.; Mitzi, D. B. Beyond 11% efficiency: characteristics of state-of-the-art $Cu_2ZnSn(S,Se)_4$ solar cells. *Adv. Energy Mater.* **2013**, *3* (1), 34−38.
(80) Mitzi, D. B.; Gunawan, O.; Todorov, T. K.; Barkhouse, D. A. R. Prospects and performance limitations for Cu-Zn-Sn-S-Se photovoltaic technology. *Philos. Trans. R. Soc., A* **2013**, *371*, 20110432.
(81) Hages, C. J.; Carter, N. J.; Agrawal, R. Generalized quantum efficiency analysis for non-ideal solar cells: Case of $Cu_2ZnSnSe_4$. *J. Appl. Phys.* **2016**, *119* (1), 014505.
(82) Altamura, G.; Vidal, J. Impact of minor phases on the performances of CZTSSe thin-film solar cells. *Chem. Mater.* **2016**, *28* (11), 3540−3563.
(83) Just, J.; Lützenkirchen-Hecht, D.; Frahm, R.; Schorr, S.; Unold, T. Determination of secondary phases in kesterite Cu_2ZnSnS_4 thin films by x-ray absorption near edge structure analysis. *Appl. Phys. Lett.* **2011**, *99* (26), 262105.
(84) Dimitrievska, M.; Xie, H.; Fairbrother, A.; Fontané, X.; Gurieva, G.; Saucedo, E.; Pérez-Rodríguez, A.; Schorr, S.; Izquierdo-Roca, V. Multiwavelength excitation Raman scattering of $Cu_2ZnSn(S_xSe_{1-x})_4$ ($0 \leq x \leq 1$) polycrystalline thin films: Vibrational properties of sulfoselenide solid solutions. *Appl. Phys. Lett.* **2014**, *105* (3), 031913.
(85) Wang, K.; Shin, B.; Reuter, K. B.; Todorov, T.; Mitzi, D. B.; Guha, S. Structural and elemental characterization of high efficiency Cu_2ZnSnS_4 solar cells. *Appl. Phys. Lett.* **2011**, *98* (5), 051912.
(86) Berg, D. M.; Arasimowicz, M.; Djemour, R.; Gütay, L.; Siebentritt, S.; Schorr, S.; Fontané, X.; Izquierdo-Roca, V.; Pérez-Rodríguez, A.; Dale, P. J. Discrimination and detection limits of secondary phases in Cu_2ZnSnS_4 using X-ray diffraction and Raman spectroscopy. *Thin Solid Films* **2014**, *569*, 113−123.

DOI: 10.1021/acsaem.8b00194
ACS Appl. Energy Mater. XXXX, XXX, XXX−XXX